Desalination and Water Treatment
www.deswater.com

doi:10.5004/dwt.2019.23822

148 (2019) 20–29
April

Hydrophobically modified silica blend PVDF nanocomposite membranes for seawater desalination via direct contact membrane distillation

Rajesha Kumar*, Mansour Ahmed, Garudachari Bhadrachari, Abbas Al-Mesri, Jibu P. Thomas

Water Research Center, Kuwait Institute for Scientific Research, P.O. Box 24885, 13109 Safat, Kuwait, email: ralambi@kisr.edu.kw (R. Kumar)

Received 5 October 2018; Accepted 22 January 2019

ABSTRACT

A simple protocol for the isolation of hydrophobically coated silica nanoparticles (HSN) by reacting tetraethyl orthosilicate (TEOS) with an excess of heptadeca- fluoro-1,1,2,2-tetrahydrodecyl) triethoxysilane is developed. The fluorinated HSN particles demonstrated a high dispersion of upto 4.0 wt% in a dope solution of 15 wt% of polyvinylidene difluoride (PVDF) in *N,N*-dimethylformamide. The nanocomposite membranes were prepared by the phase inversion technique with a casting thickness of 150 µm. PVDF-HSN membranes witnessed an improved porosity and hydrophobicity compared to the neat PVDF membrane. The membrane morphological, contact angle, roughness, and liquid entry pressure studies demonstrated a suitable modification of membranes in favor of membrane distillation (MD) application. The MD performance was tested in direct contact membrane distillation configuration for the hot feed of Arabian Gulf seawater with a TDS of 35,800 ppm, and cold deionized water as permeate. Though, the loading of HSN above 3.0 wt% produced more hydrophobic membrane surfaces, the loading of 3.0 wt% of HSN was settled as an optimized composition to attain high performance during MD. The maximum transmembrane permeate flux of 42.32 kg/m^{2}h with total salt rejection was obtained for 3.0 wt% loading of HSN when feed and distillates temperatures were at 80°C and 20.0°C, respectively.

Keywords: Nanocomposite; Membrane fabrication; Membrane distillation; Membrane morphology; Nanomaterials

1. Introduction

Membrane distillation (MD) has gained much attention across the globe as an efficient technology for the extraction of pure water from seawater and concentrated brine discharge. MD technology works on the principle of transport of water vapors through a porous and hydrophobic membrane by maintaining a temperature difference across the membrane [1]. The development of membranes for MD application comprises a proper selection of polymeric material is desired to achieve a membrane surface with a high porosity and good hydrophobicity to avoid the membrane wetting during the operations. The most commonly employed polymers for membrane fabrication are polyvinylidene difluoride (PVDF), polypropylene (PP) and polytetrafluoroethylene (PTFE).The PVDF based membranes could be easily fabricated using non-solvent induced phase separation due to its solubility in common polar organic solvents [2]. While the melt extrusion techniques are quite commonly employed for the fabrication of PP and PTFE membranes due to their solubility issues [3].

PVDF polymer as a neat membrane material lack from sufficient porosity and hydrophobicity for MD application. Therefore, several methods have been developed in the literature to improve the characteristics of PVDF membranes for MD application. The incorporation of hydrophobic nanomaterials as a nanofillers either by blending

*Corresponding author.

or by coating are the interesting options to improve PVDF membrane performance [4]. The hydrophobic nanoparticles have great influence on the improved membrane morphological features, porosity, pore size, and hydrophobicity in favor of MD application [5]. The silica (Si) nanoparticles demonstrate a facile protocol for the hydrophobic modification due to the presence of reactive –OH groups and quite commonly employed modification method include fluorination reaction using different derivatives of triethoxy silanes [6–9]. The incorporation of fluoro Si into the PVDF membrane matrix revealed an interesting option to attain improved permeation and long-term stability during MD experiments. Zhao et al. 2017 developed a facile surface modification method to obtain hydrophobic PVDF membranes by depositing fluorographite particles on the membrane surface [10]. The wetting resistance of the membrane surfaces increased with the increase in a number of fluorographite particles on the membrane surface. A better performance, sustainability in DCMD tests was achieved using a highly concentrated sodium chloride (10 wt%) solution as feed. Lu et al. developed the amphiphobic PVDF composite membranes for MD with excellent tolerance to various organic foulants [11]. An easy surface modification method was explored by dynamically forming perfluorooctyl trichloro silane (PFTS) and coating SiO_2 nanoparticles onto the PVDF membrane surface. The anti-fouling, anti-wetting properties of the surface modified membranes improved along with the stable operations during the DCMD trials.

The membranes prepared by the blending of nanoparticles has advantages over coating technique, where the former technique allows the insertion of nanoparticles into the bulk of membrane matrix [12]. The incorporation of highly dispersible hydrophobic nanoparticles alters the membrane morphological features in favor of MD application. Sebastian et al. fabricated the high flux, robust membranes for the purification of artificial seawater by incorporating graphene oxide functionalized with 3-(aminopropyl) triethoxysilane (APTS) into PVDF polymer solutions [13]. The addition of graphene oxide (GO) and GO-APTS enhanced the permeate flux by 52% and 86%, respectively, compared to pure PVDF. The best performing membrane contained 0.3 wt% GO-APTS (with respect to PVDF) and had a flux of 6.2 LMH (L $m^{-2}h^{-1}$) whilst maintaining perfect salt rejection (>99.9%). These improvements were attributed to increased surface and bulk porosity, larger mean pore size and hydrophilic. Mohamed et al. prepared multi-walled carbon nanotube (MWCNT), silicon dioxide (SiO_2), titanium dioxide (TiO_2) and zinc oxide (ZnO) doped polysulfone (PSf) flat sheet membranes was by phase inversion process [14]. The highest permeate flux obtained in the order of MWCNT (41.58) > SiO_2 (38.84) > TiO_2(35.6) >ZnO (34.42 L/m^2h) with optimized concentration of 1.0, 0.5, 0.75, 0.5 wt% relative to PSf weight, i.e. 15%. The optimum operational conditions included feed and permeate temperatures 60°C and 20°C, respectively, synthetic NaCl feed water with salinity was 10,000 ppm. Hou et al. prepared poly(vinylidene fluoride-co-hexafluropropylene) (PVDF-HFP)/Silica nanoparticles (SiNPs) flat-sheet hybrid membranes for membrane distillation via electrospinning, and the effects of SiNPs on the properties of the resultant membranes were investigated [15]. The SiNPs addition enlarged the pore diameter and the liquid entry pressure of water of the hybrid membrane was not significantly influenced by the SiNPs addition. The membranes were tested through direct contact membrane distillation using 35 g/L NaCl solution as feed, and the highest permeate flux bout 48.6 kg/m^2 h was obtained and the salt rejection maintained 99.99%. The membrane hydrophobicity can also maintain well with long-time immersion in salt solution. A novel PVDF blend nanocomposite membrane to enhance the flux and wetting resistance of PVDF membranes for MD applications was prepared using a polystyrene/ZnO (PS/ZnO) hybrid nanocomposite [16]. It was found that the addition of the PS/ZnO hybrid nanocomposite (0.25, 0.5 and 0.75%) resulted in an increase in porosity (>70%) due to increased pore size and reduction of the spongy layer thickness. Furthermore, the addition of the nanocomposite also improved the surface roughness and contact angle. The membranes composed of 0.75% PS/ZnO hybrid nanocomposite exhibited high performance stability and the desalination flux of 30 g L^{-1} saline aqueous solution significantly increased, and rejection reached 99.99%.

The favorable morphological characteristics of MD membranes include a sponge-like structure than a finger-like structure for the improved porosity and mechanical property [17,18]. Sun et al. reported the formation of the finger-like upper layer and the sponge-like bottom layer by the blending of polydimethylsiloxane with PVDF [19]. With the increase of PDMS in the dope solution, the length of the finger-like layer reduced, and the loose spongy pores fully distributed over the membrane cross sections. The altered morphological features, especially with more sponge-like structures, were achieved by a uniform and high dispersion of nanoparticles in the dope solution. The spongy structures were formed due to the lowered rate of precipitation during the phase inversion process in the presence of nanoparticles [20,21]. The reformed morphological structures with increased spongy pores by the incorporation of nanoparticles was consistent with the few other MD studies [22,23].

In this current work, we demonstrate a novel process for the isolation of hydrophobically modified silica nanoparticles (HSN) by coating a long chain fluoro derivative of triethoxy silane. The coated particles were segregated in the reaction mixture itself by adding an excess of heptadeca-fluoro-1,1,2,2-tetrahydrodecyl) triethoxysilane (HDFTT) as a reagent. The HSN nanoparticles were characterized and used as filler for the fabrication of PVDF nanocomposite membranes. The seawater desalination of newly fabricated PVDF-HSN membranes was tested in direct contact membrane distillation configuration. Also, this study covers the detailed characterization of PVDF-HSN membranes to correlate the membrane structural features with the desalination performance results.

2. Materials and methods

The polymer PVDF Kynar® HSV 900 powder (specific gravity: 1.76–1.79, tensile strength at yield (MPa), tensile elongation at yield (5–10%) was acquired from Arkema Inc. HDFTT was purchased from ABCR GMBH, Germany, Tetraethylorthosilicate and polyethylene glycol (M_w = 600 Da) were procured from Sigma Aldrich Co., ethanol, sodium chloride, and 25% solution of aqueous ammonia were purchased from Merck Co.

2.1. Synthesis of fluoro coated silica nanoparticles (HSN)

The synthesis of HSN includes a reported protocol in the literature with modifications in the stoichiometric ratio of the reactants [24]. In the modified protocol the excess addition of HDFTT allowed the settling of precipitated fluoro coated Si in the reaction mixture itself. In a typical procedure, tetraethyl orthosilicate (20 mL), with an excess of HDFTT (10 mL) was dissolved in 100 mL of ethanol at 25–26°C. Then the reaction mixture was charged with a solution of ammonium hydroxide/ethanol solution (25 ml 28% $NH_3{\cdot}H_2O$ in 75 mL ethanol) at 25–26°C. The turbid solution was allowed to stir at 25–26°C for 12 h to ensure complete fluoro coating of the Si nanoparticles. The stirring was stopped to settle down the precipitated HSN particles, the supernatant was separated by decanting, the precipitates were washed with ethanol (2×100 mL) followed by washing with deionized water (1×100 mL) and dried at 80°C for 5 h.

2.2. Preparation of membranes

PVDF (15.0 wt%) was dissolved in *N, N*-Dimethylformamide (82.0 wt%) and polyethylene glycol (3.0 wt%) over a period of 10 h at 50°C. The dope solution was allowed to stand at 50°C for 1 h to eliminate the trapped air bubbles. Then, the dope solution was cast over a polyester non-woven fabric support using a casting blade adjusted to a thickness of 150 µm. Finally, the membrane was precipitated by dipping the coated fabric support in deionized water at 25–26°C. So, the obtained membrane was washed several times with the DI water and dried at 25–26°C before characterization. The PVDF membranes with HSN fillers were prepared using the similar protocol and their compositions as presented in Table 1.

2.3. Membrane characterization

2.3.1. FTIR analysis

The FTIR of HSN was recorded using ATR-IR instrument from Bruker Co. (ALPHA model) to confirm the chemical modification of silica nanoparticles by fluoro coating.

2.3.2. Membrane morphological study

FESEM from Keysight technologies (model-1500) was used for the membrane surface and cross-sectional images in backscattering mode, to characterize HSN particles and to take Energy dispersive spectrum of the PVDF-3.0HSN membrane. The surface roughness of the membranes was recorded using AFM instrument from Concept Scientific Instrument (Nano-Observer), France, by scanning the membrane surface over 10 × 10 µm dimensions.

2.3.3. Contact angle measurement

The membrane surface hydrophobicity was evaluated by contact angle measurements using an optical contact angle and interface tension meter from USA KINO (model-SL200KB).

2.3.4. Liquid entry pressure (LEPw) measurement

The LEPw values of membranes were measured using a dead-end filtration cell purchased from Sterlitech Corporation, USA. The pressure of the feed side slowly increased at a 0.05 MPa interval during the measurement. At each pressure interval, the membrane was kept at the constant pressure for 10 min and the pressure was noted when the first drop of water came from the cell permeate side [25]. This pressure was considered as a LEPw point.

2.3.5. Porosity and pore size measurement

The porosities of membranes were determined according to the gravimetric method [22]. The initial weight of the wetted membrane in anhydrous isopropanol was recorded as m_1 after immersing the sample for 24 h. Then, the wetted sample was dried in an oven at 50°C for 24 h and the dry weight of the membrane was recorded as m_2. The overall porosity of the membrane was recorded using the following equation:

$$\varepsilon = \frac{\left(m_1 - m_2\right)/\rho_w}{\left(m_1 - m_2\right)/\rho_w + m_2/\rho_P} \quad (1)$$

where m_1 is the weight of the wet membrane, m_2 is the final weight of dried membranes, ρ_w is the density of isopropanol (0.786 g/cm^3) and ρ_p is the density of the polymer (1.78 g/cm^3).

The FESEM instrument was used to determine the pore size of the top surface of the membranes assuming that the surface pores were circular [26–28]. The average pore size was reported by selecting average 50 pores randomly from each membrane sample.

Table 1
The codes, compositions of synthesized membranes and their physical properties

Membrane Code	PVDF (wt%)	DMF (wt%)	PEG (wt%)	HSN (wt%)	Dope viscosity (Pa.s)	Contact angle (°)	LEPw (kPa)	Porosity (%)	Pore size (nm)
PVDF	15.0	82.0	3.0	0.0	3.8	68.6	85	53.6	52
PVDF-1.0HSN	15.0	81.0	3.0	1.0	4.7	74.9	98	66.1	54
PVDF-2.0HSN	15.0	80.0	3.0	2.0	5.8	78.8	115	68.3	55
PVDF-3.0HSN	15.0	79.0	3.0	3.0	6.9	85.1	130	71.1	56
PVDF-4.0HSN	15.0	78.0	3.0	4.0	9.2	88.4	110	70.2	62

2.4. Flux and mass transfer coefficient calculations and DCMD test protocol

For MD performance of the PVDF and PVDF-HSN membranes were tested in a custom-made multiconfiguration MD test unit from Convergence Instruments. The flow sheet diagram of the MD system is presented in Fig. 1, and performance of the membranes was evaluated in direct contact membrane distillation configuration. The system included in-line temperature sensors, pressure sensors, pH and conductivity sensors, flow sensors and weighing balances to monitor temperature, pressure, pH, salinity flow and weights, respectively, on feed and permeate sides. The system has a dosing system to dose water to keep the concentration constant at the feed side or dynamically increase or reduce the salinity. The heating of the system was done via plate and frame heat exchangers that are connected to a heating or chilling bath. All tubing and connectors are corrosion resistant, including flow through blocks for the sensors. All tubing from the hot and cold side are thermally insulated to keep heat loss to a minimum. The cold side was cooled via either the available chilled water line or an already available chiller unit. The system was fully automated with software which allows to build/customize experiments and create MS Word/Excel/PDF results. The system has highly flexible and suitable to fit any flat sheet membrane module. In a typical procedure of DCMD experiment, the flat-sheet membrane 50 mm (diameter) was tightly clamped between the two chambers of the membrane module. The hot feed of real seawater collected from beach well of a desalination plant at Doha, Kuwait and cold DI water as permeate were flowed concurrently from the bottom to the upper part of the module with the help of two pumps. The initial volume of the feed and the distillate were 2.0 L and 0.25 L, respectively. The circulation feed rate and permeate rate were adjusted by using two electromagnetic flow meters. The fluid temperatures were controlled by water baths and monitored at the inlet and outlet of the module using temperature sensors (with scale –20°C to 120°C). The experiments were carried out under different feed temperatures in the range of 50–80°C over a period of 180 min,while the inlet temperature of the cold water was kept constant at 20°C. For each membrane, three different experiments were conducted using similar experimental conditions and the average flux and rejection values have been reported. The permeate flux of the membrane was calculated by the following equation:

$$J = \frac{\Delta W}{A\Delta t} \tag{2}$$

where J is the permeate flux (kg/m² h), ΔW is the quantity of distillate (kg), A is the effective membrane area (m²) and Δt is the sampling time (h).

The water vapor flux (J_w) in MD can also be expressed by Eq. (3) and it is used to determine the mass transfer coefficient [29].

$$J_w = k\left(P_f - P_p\right) \tag{3}$$

where k is the mass transfer coefficient which can be rearranged as Eq. (4)

$$k = \frac{J_w}{\left(P_f - P_p\right)} \tag{4}$$

where P_f and P_p are the partial water vapor pressure in feed and permeate side respectively.

2.5. Water quality analysis

Total dissolved solids (TDS) of seawater feed and permeate were measured by Thermo Scientific instrument. The pH and conductivity were measured by SI analytics instrumentation. The other parameters such as calcium, magnesium, chloride, and sulphate were assessed by ion chromatography system (ICS), whereas, boron and sodium are determined by inductively coupled plasma optical emission spectrometry (ICP-OES). The parameters such as silica, phosphate, and fluoride are estimated by spectrophotometer (DR-6000). All analysis was done in triplicate and average values were reported.

3. Results and discussion

3.1. FTIR analysis

The FTIR spectrum of HSN displayed a peak at 1200 cm^{-1} corresponding to the C-F stretching [30,31]. The peak at 1085 cm^{-1} and 804 cm^{-1} at (Fig. 2) attributed to the Si-O-Si

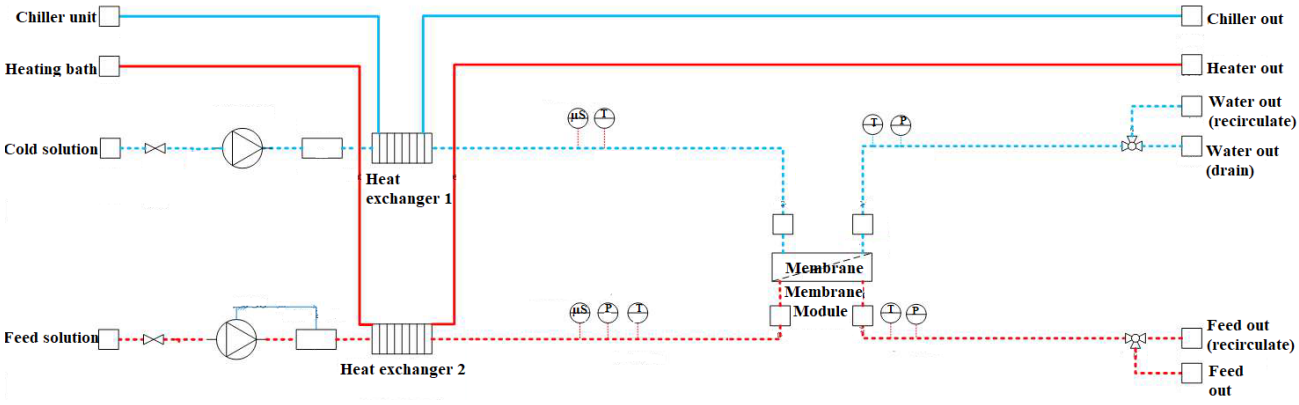

Fig. 1. Schematic diagram of the membrane distillation test unit.

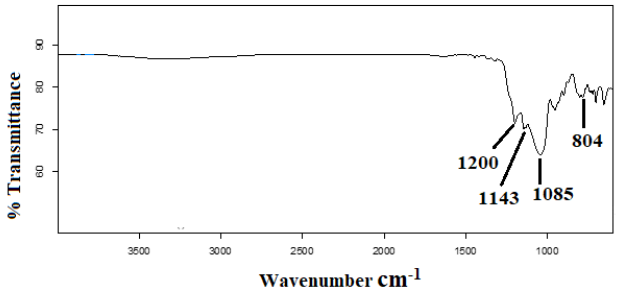

Fig. 2. The FTIR spectrum of HSN.

stretching [32]. The characteristic peak of silica coating appeared at 1,143 cm^{-1} corresponding to Si-O-C bond, which confirms that the $-(CH_2)_2-(CF_2)_7-CF_3$ molecules are clearly attached to silica nanoparticles [7].

3.2. FESEM analysis

The FESEM image of HSN revealed the formation of nano-sized particles with a varying size in the range of 30–80 nm (Table 1). Fig. 3 represents the surface and cross-sectional images of the neat PVDF and PVDF-HSN membranes. The cross-sectional views of all the membranes

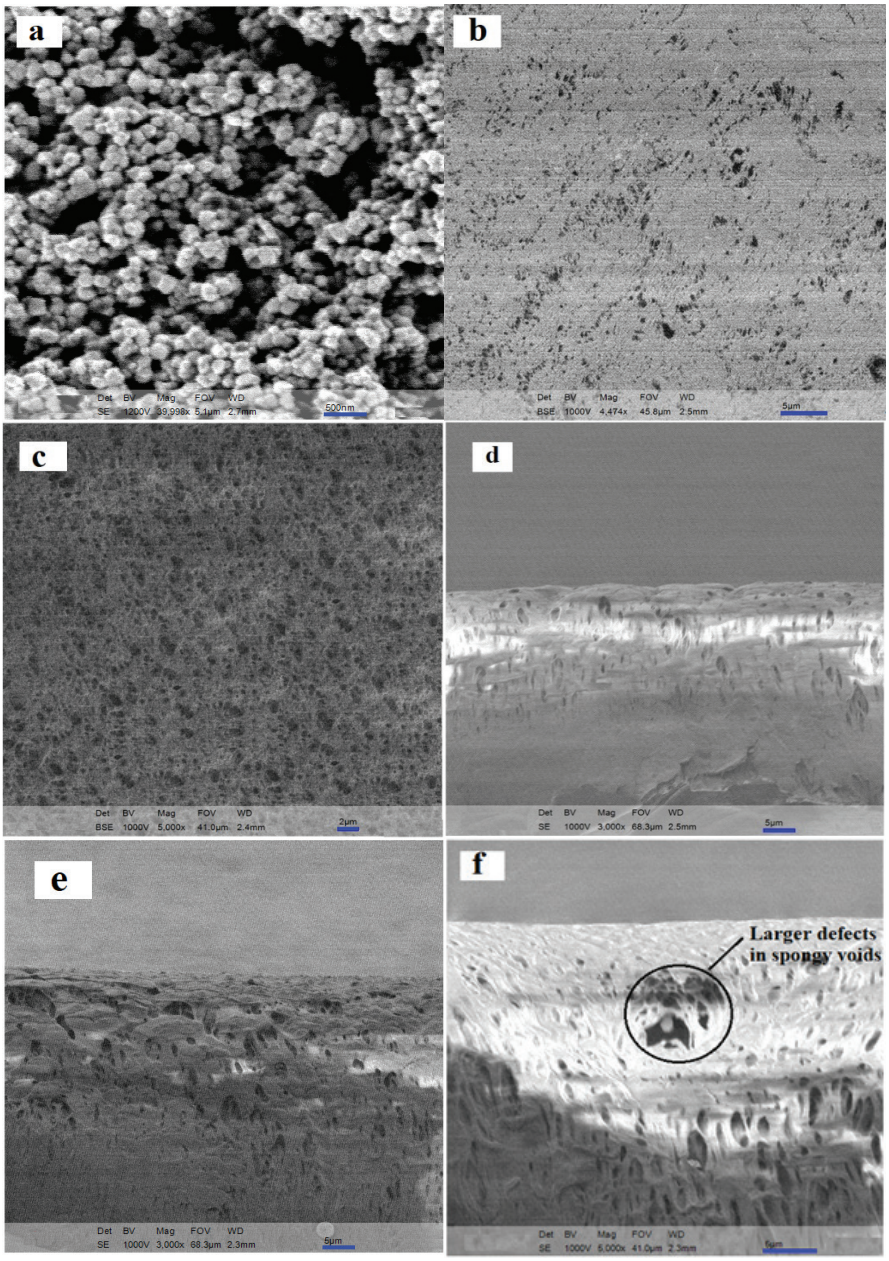

Fig. 3. FESEM images of a) HSN nanoparticles, b and c) surfaces of PVDF and PVDF 3.0HSN-membranes, d, e, and f) cross-sectional images of PVDF, PVDF-3.0HSN and PVDF-4.0HSN membranes respectively.

presented the asymmetric structures of membranes with a dense top layer and a sublayer with porous structures. It is well evidenced by the previous literature that the presence of a sponge-like structures in the sublayer relatively produces more porous membranes [7,20,33]. As an important requirement of MD membrane morphological characteristics, the addition of HSN suppressed the rate of precipitation during the phase inversion process and generated more sponge type structures in the sublayer [34]. The loading of HSN in increasing concentration was the reason for the conversion of larger finger-like voids to short spongy structures in the membrane cross-sections. Generally, the addition of hydrophilic nanoparticles to the casting solution increase the penetration of water molecules more deeply into the membrane matrix to generate finger-like voids [23]. In contrary, the nanoparticles selected in the study are hydrophobic due to the coating of fluoro functional groups. Therefore, the formation of fully spongy structures for the higher loading of HSN is ascribed to the water-repellent HSN molecules which might show resistance for the easy entry of non-solvent water molecule into the depth of cast film. The energy dispersive spectral analysis of the PVDF-3.0HSN membrane (Fig. 4) confirmed the successful loading and accumulation of the fluoro modified silica particles onto the membrane surface. Overall, the membrane morphology was altered from finger-like voids to spongy structures as an essential feature towards the MD application.

3.3. Liquid entry pressure, contact angle, porosity and dope viscosity

The fluorination is the common method to be used to lower the surface free energy of the silica particles for the improved hydrophobicity [35]. Also, the small radius and a high electronegativity of Fluorine makes the bonding interaction between fluorine and carbon more stable. In the current work, the increase in the number of fluorine linked carbon chains to the silica particles has lowered the surface energy and increased the surface contact angle values [36]. Additionally, the modification of silica particles by long-chain $–CF_2$ groups and their presence on the membrane surface had poor adhesion for water molecules due to the weak van der Waals force [37]. The contact angle values of the PVDF-HSN membranes increased to a maximum of ~88 ° for the loading of 4.0 wt% of nanofiller. LEPwin membrane distillation signifies the resistance offered towards the wettability by the membrane surface to overcome the hydrophobic forces and to penetrate the membrane pores. Therefore, the LEPw value should be high for ideal MD membrane to attain long-term performance. The PVDF membranes modified by loading of HSN produced higher LEPw values due to altered pore morphology and hydrophobicity values [38]. The contact angle values of PVDF-HSN membranes increased with the increased loading of HSN as shown in Table 1. All the PVDF-HSN membranes attained contact angle values less than 90°, thus the pore morphology has contributed much towards the improved LEPw values. The LEPw values as presented in Table 1 was increased for the loading of HSN upto 3.0 wt% due to the formation of smaller spongy voids in the sublayer. Thereafter, the loading of 4.0 wt% HSN lowered the LEPw due to the formation of defected larger voids within sponge type structures in cross-sections (Fig. 3f). Therefore, loading of HSN up to 3.0 wt% favored the formation of appropriate pore structures to attain high LEPw values. Altogether, the loading of HSN favored the formation of more hydrophobic membrane surface and increased the LEPw values to achieve higher anti-wetting property during MD. Also, the porosity values presented in Table 1 revealed the increased porosity of PVDF-HSN membranes until a loading of 3.0 wt% of HSN, attributed to the better dispersion of HSN as presented in Fig. 5. The improved porosity of PVDF-HSN membranes could be the other reason for the moderate increase in contact angle values of the PVDF-HSN membranes [39]. The viscosity data presented in Table 1 revealed a drastic increase in viscosity for PVDF-4.0HSN dope solution due to the excess loading of HSN having high surface energy resulted in the agglomeration of particles. The increased viscosity for PVDF-4.0HSN had a negative impact on both LEPw and porosity values of the resultant membrane due to the agglomeration of HSN in the dope solution. However, the loading of HSN upto 3.0 wt% has

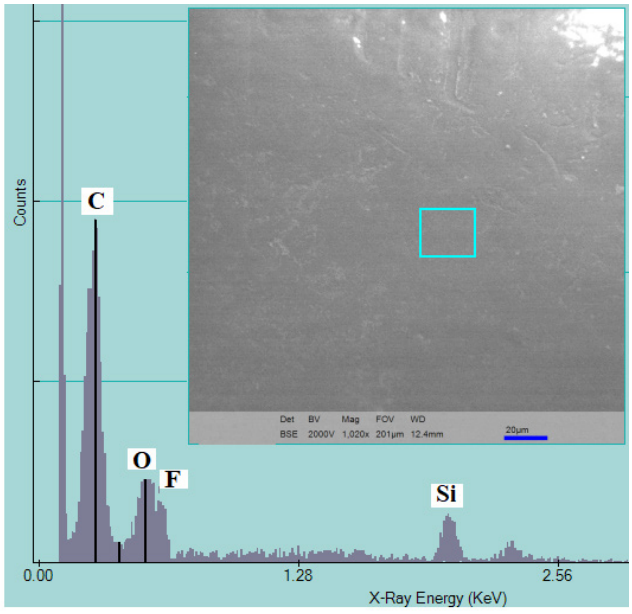

Fig. 4. Energy dispersive X-ray spectrum of PVDF-3.0 HSN membrane surface.

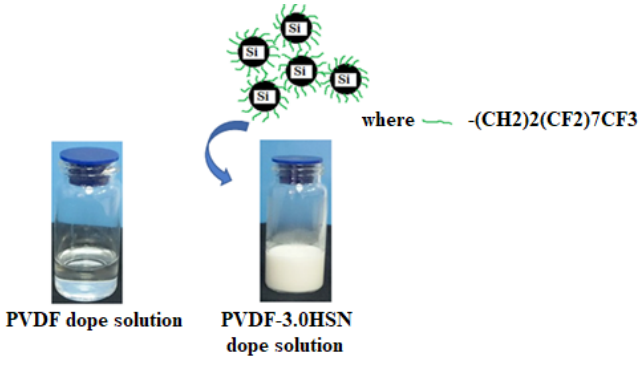

Fig. 5. The images of PVDF and PVDF-3.0HSN dope solutions.

positive influence on the increased porosity and hydrophobicity of the membranes essential for MD application.

3.4. AFM analysis

The AFM 3D images of membranes with their average roughness are presented in Fig. 6. The roughness parameters of PVDF-HSN membranes were greatly influenced by the loading of HSN nanoparticles. Generally, during the incorporation of fluorinated silica nanoparticles, the driving force for the formation of the superhydrophobic surface comes from an agglomeration of nanoparticles onto the substrate to form a rough surface with a low free energy [24]. Consequently, during the formation of PVDF-HSN membranes via the phase inversion process, the hydrophobic HSN nanoparticles partly leached into the coagulation medium. However, due to the less affinity HSN towards water, some part of HSN retained on the membrane surface to attain rough surfaces for PVDF-HSN membranes. The loading of 4.0 wt% of HSN produced a highest average surface roughness of 620 nm and this composition corresponds to the maximum agglomeration of HSN on the membrane surface producing more ridges and valley structures [40]. Additionally, the introduction of long fluorine chains created rougher surfaces on the membrane surface, and this played a positive role in hydrophobicity by decreasing the surface free energy as well. The porosity data also supported this observation which showed less porous structures for the PVDF-4.0HSN membrane of particle agglomeration at higher concentration. However, a control over increased roughness was achieved until a loading of 3.0 wt% of HSN. The loading of 3.0wt% of HSN termed as an optimized composition of loading to attain good dispersion of nanoparticles and valid roughness values.

3.5. Effect of HSN on permeation flux and performance

The permeate flux of PVDF and PVDF-HSN membranes at 50–80°C are presented in Fig. 7. The permeate flux of all the membranes increased with the increase in temperature due to the increased water vapors as the driving force of the process. Also, the permeate flux of PVDF-3.0HSN membrane was increased to 42.32 kg/m²h with a rejection of >99.0% towards seawater TDS and its rejection for other seawater chemical parameters are presented in Table 2. The physiochemical analysis of the permeate obtained for

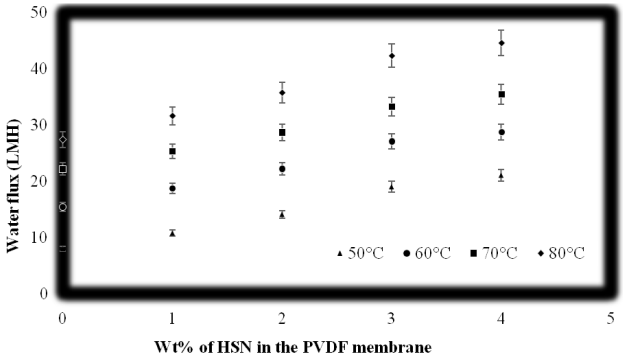

Fig. 7. The water flux of membranes at different temperatures.

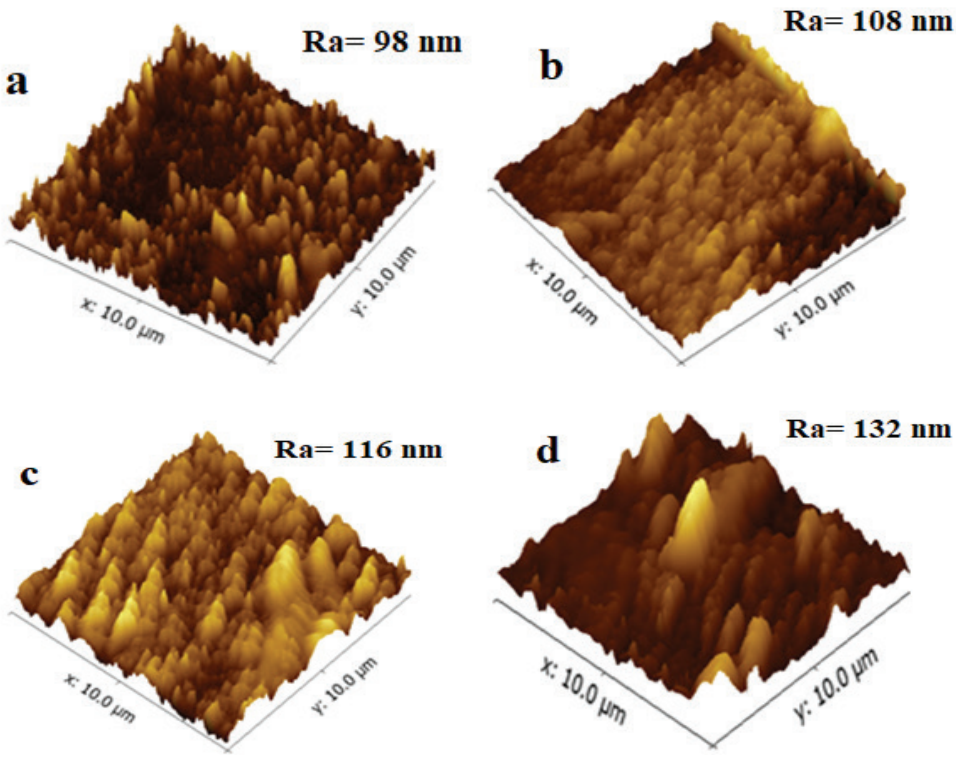

Fig. 6. AFM 3D images of a) PVDF, b) PVDF-1.0HSN, c) PVDF-3.0HSN and d) PVDF-4.0HSN membranes.

Table 2
Physiochemical analysis of Arabian gulf seawater feed and permeate obtained for PVDF-3.0HSN and PVDF membranes at 80°C

Parameter	Seawater feed	Permeate (PVDF)	Permeate (PVDF-3.0HSN)
pH	7.4	7.1	7.1
Conductivity, mS/cm	55.4	0.32	0.31
TDS, ppm	35800	161	154
Calcium, mg/L	824	10.4	8.16
Magnesium, mg/L	1154	7.1	6.23
Sulfate, mg/L	3600	25	21
Chloride, mg/L	26000	34	28
Sodium, mg/L	14,800	98	85
Boron, mg/L	2.75	0.20	0.14
Nitrate, mg/L	3.5	0.75	0.7
Silica, mg/L	16.2	0.903	0.724
Phosphate, mg/L	0.15	0.14	0.11
Fluoride, mg/L	4.3	0.17	0.13

PVDF and PVDF-3.0HSN membranes has been presented in Table 2. A slightly higher rejection offered by the PVDF-3.0HSN towards Si might be due to the electrostatic repulsive interaction between the Si present in seawater and the HSN already present on the membrane surface. The loading of 4.0 wt% of HSN corresponds to a maximum permeate flux of 44.6 kg/m²h at 80°C, however, its salt rejection value was dropped from 99.99% to 96.8% due to the formation of defected structures in the membrane due to particle agglomeration effect. Therefore, the loading composition of HSN played a crucial role in determining the optimum performance of the PVDF-HSN based membranes. As revealed from the membrane morphological study the formation of more spongy structures for the loading of 3.0wt% of HSN has increased the membrane flux. Generally, the membrane with a smooth surface displays the superior flux than the rougher surface [41]. However, as revealed in Fig. 8 the increased roughness for the PVDF-HSN membranes was quite less for the loading of HSN up to 3.0 wt% and consequently had less effect on the flux. The improved flux of the PVDF-HSN membranes could be explained by the formation of the more channels for the transport of water vapor molecules by the loading of HSN as evidenced from the surface FESEM images and porosity data. Also, PVDF-3.0HSN membrane durability was tested at 80°C and membrane showed its superior anti-wetting property over a long run of 200 h. The drop-in flux was to 41.1 kg/m²h from its initial value of 42.32 kg/m²h with a minor drop in rejection to >98.5% towards seawater TDS demonstrating the stable performance of the membrane over a period of 200 h. A comparative study revealed that PVDF-3.0HSN membrane had ~3 times higher durability than the neat PVDF membrane, where the later witnessed salt leakage at around 70 h of operation. The contact angle study was repeated for the PVDF-3.0HSN and neat PVDF membranes after the long run experiments by washing the membranes using DI water followed by drying. The PVDF-3.0HSN membrane showed almost a stable contact angle of 84.9° after 200 h of operation attributed to the good compatibility between HSN and PVDF polymer matrix not allowing the easy washing of HSN particles during the MD experiment. Whereas, the contact angle of neat PVDF reduced to 54.3° after 70 h of operation and the membrane witnessed easy wetting and salt leakage during the MD experiment.

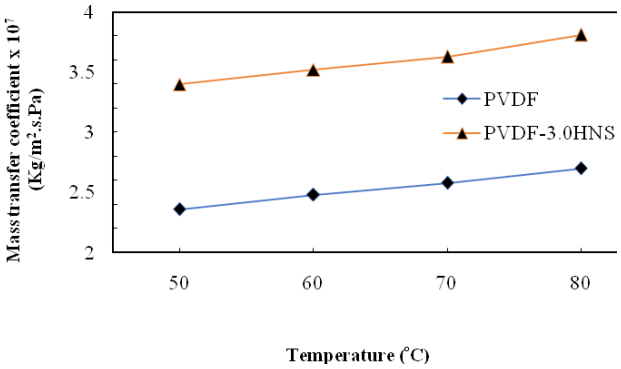

Fig. 8. Effect of temperature on mass transfer coefficient of neat PVDF and PVDF-3.0HSN membranes.

The vapor pressure as a main driving force of the MD process tends to increase with the increase in the operating temperature of the feed stream. As presented in Fig. 8, the overall mass transfer coefficient for both the control PVDF and PVDF-3.0HSN membranes is increased slightly with an increase in temperature due to the increase in the rate of water vapor diffusion. At any temperature, the PVDF-3.0HSN membrane showed higher mass transfer coefficient compared to the neat PVDF membrane (illustrated in Fig. 8) attributed to the increased porosity of the PVDF membranes by HSN particles. The enhancement in the mass transfer coefficient could also be due to the lowered internal heat loss through the membrane containing the hydrophobic fluoro silica particles especially in DCMD configuration [42].

4. Conclusions

The current study developed a new synthetic protocol for the isolation of fluoro coated silica nanoparticles (HSN). The synthesized HSN particles were hydrophobic and demonstrated a good dispersion in PVDF dope solution to fabricate PVDF-HSN membranes. The contact angle study revealed the contribution of HSN particles towards the improved wetting resistance of the PVDF-HSN membranes in favor of MD application. The less affinity of HSN towards water molecules resulted in the retarded phase inversion process and formed more spongy structures with reduced pore size. The loading of hydrophobic HSN into PVDF matrix at appropriate composition revealed its potentiality to apply in MD application. The formation of spongy structures for PVDF-3.0HSN membrane contributed to the higher porosity of the membrane to attain a high flux of 42.32 kg/m²h and displayed stability over 70 h of operation.

Acknowledgement

Authors are thankful to the Kuwait Foundation for Advancement of Sciences for partly funding this proj-

ect and Kuwait Institute for Scientific Research (KISR) for financially supporting this research activity.

List of Abbreviations

AFM	—	Atomic force microscope
APTS	—	3-(aminopropyl) triethoxysilane
ATR-IR	—	Attenuated total reflectance infra-red
DCMD	—	Direct contact membrane distillation
FTIR	—	Fourier transform infrared
GO	—	Graphene oxide
HSN	—	Hydrophobically coated silica nanoparticles
ICP-OES	—	Inductively coupled plasma optical emission spectrometry
ICS	—	Ion chromatography system
LEP	—	Liquid entry pressure
MD	—	Membrane distillation
MWCNT	—	Multi walled carbon nanotube
MWCNT	—	Multi-walled carbon nanotube
PP	—	Polypropylene
PS	—	Polystyrene
PSf	—	Polysulfone
PTFE	—	Polytetrafluoroethylene
PVDF	—	Polyvinylidinefluoride
PVDF-HFP	—	Poly (vinylidene fluoride-co-hexafluropropylene)
SEM	—	Field emission scanning electron microscope
SiNPs	—	Silica nanoparticles
TDS	—	Total dissolved solids
TEOS	—	Tetraethyl orthosilicate

References

[1] A. Abdullah, D. Naif, H. Nidal, Membrane distillation: A comprehensive review, Desalination, 287 (2012) 2–18.
[2] G. Ferreira, V.F. Cardoso, A.C. Lopes, G. Botelho, S. Lanceros-Méndez, Tailoring microstructure and physical properties of poly (vinylidene fluoride–hexafluoropropylene) porous films, J. Mat. Sci., 50 (2015) 5047–5058.
[3] Zhongde, A. Luca, D. Liyuan, Recent advances in multi-layer composite polymeric membranes for CO_2 separation: A review, Green. Ener. Environ., 1 (2016) 102–128.
[4] L. Xuemei, P. Yuelian, G. Lei, L. Rijia, Z. Zhonghua, L. Shaomin, Amphiphobic PVDF composite membranes for anti-fouling direct contact membrane distillation, J. Membr. Sci., 505 (2016) 61–69.
[5] Hou, G. Dai, H. Fan, J. Wang, C. Zhao, H. Huang, Effects of calcium carbonate nano-particles on the properties of PVDF/nonwoven fabric flat-sheet composite membranes for direct contact membrane distillation, Desalination, 347 (2014) 25–33.
[6] W. Feng, Z. Huapeng, Z. Hailin, G. Yuhai, Ultra-hydrophobic modification of TiO_2 nanoparticles via thermal decomposition of Polytetrafluoroethylene, Powder Technol., 253 (2014) 548–552.
[7] B. Jean-Denis, D.K. Sarkar, P. Jean, Fluorine based superhydrophobic coatings, Appl. Sci., 2 (2012) 453–464.
[8] Yongqin, W. Di, J. Xin, X. Bosong, Synthesis and characterization of fluorinated organic–inorganic hybrid coatings on tinplate, J. Appl. Polym. Sci., 132 (2015) 42428.
[9] M. Peng, Z. Liao, Z. Zhu, H. Guo, H. Wang, Fumed silica/polymer hybrid nanoparticles prepared by redox-initiated graft polymerization in emulsions, J. Mat. Sci., 44 (2009) 6286–6293.
[10] D. Zhao, J. Zuo, K-J. Lu, T-S. Chung, Fluorographite modified PVDF membranes for seawater desalination via direct contact membrane distillation, Desalination, 413 (2017) 119–126.
[11] X. Lu, Y. Peng, L. Ge, R. Lin, Z. Zhu, S. Liu, Amphiphobic PVDF composite membranes for anti-fouling direct contact membrane distillation, J. Membr. Sci., 505 (2016) 61–69.
[12] X. Yang, Y. He, G. Zeng, Y. Zhan, Y. Pan, H. Shi, Q. Chen, Novel hydrophilic PVDF ultrafiltration membranes based on a ZrO_2–multiwalled carbon nanotube hybrid for oil/water separation, J. Mat. Sci., 51 (2016) 8965–8976.
[13] L. Sebastian, A-K. Ahmed, F. Bilal, M.L-A. Jose, A. Monica, V. Aravind, M.H. Stuart, S. Gyorgy, I.B. Mohamed, S. Nima, G. Patricia, Flux-enhanced PVDF mixed matrix membranes incorporating APTS-functionalized graphene oxide for membrane distillation, J. Membr. Sci., 554 (2018) 309–323.
[14] S.F. Mohamed, M.A. Abdel-Hameed, M.A. Mustafa, S.O. Adel, D. Rasel, Comparative performance evaluations of nanomaterials mixed polysulfone: A scale-up approach through vacuum enhanced direct contact membrane distillation for water desalination, Desalination, 451 (2019) 111–116.
[15] H. Deyin, L. Dichu, D. Chunli, W. Dewu, W. Jun, Fabrication and characterization of electrospun superhydrophobic PVDF-HFP/SiNPs hybrid membrane for membrane distillation, Sep. Purif. Technol., 189 (2017) 82–89.
[16] R. Ramin, A. Fatemeh, P. Majid, J. Mohsen, Highly permeable PVDF membrane with PS/ZnO nanocomposite incorporated for distillation process, RSC Adv., 8 (2018) 23499–23515.
[17] T.H. Young, L.W. Chen, Pore formation mechanism of membranes from phase inversion process, Desalination, 103 (1995) 233–247.
[18] J.F. Li, Z.L. Xu, H. Yang, Microporous polyethersulfone membranes prepared under the combined precipitation conditions with non-solvent additives, Polym. Adv. Technol., 19 (2008) 251–257.
[19] S. De, L. Mei-Qin, G. Jun-Heng, Z. Jin-Yan, L. Bing-Bing, L. Da-Yong, Preparation and characterization of PDMS-PVDF hydrophobic microporous membrane for membrane distillation, Desalination, 370 (2015) 63–71.
[20] P.V. Witte, P.J. Dijkstra, J.W.A. van den Berg, J. Feijen, Phase separation processes in polymer solutions in relation to membrane formation, J. Membr. Sci., 117 (1996) 1–31.
[21] L. Sebastian, A-K. Ahmed, F. Bilal, M.L. Jose, A. Monica, V. Aravind, M.H. Stuart, S. Gyorgy, I.B. Mohamed, S. Nima, G. Patricia, Flux-enhanced PVDF mixed matrix membranes incorporating APTS-functionalized graphene oxide for membrane distillation, J. Membr. Sci., 554 (2018) 309–323.
[22] T.L.S. Silva, S. Morales-Torres, J.S. Figueiredo, A.M.T. Silva, Multi walled carbon nanotube/PVDF blended membranes with sponge- and finger-like pores for direct contact membrane distillation, Desalination, 357 (2015) 233–245.
[23] B. Mohammadali, R. Dipak, M. Takeshi, Q.L. Christopher, Effects of hydrophilic CuO nanoparticles on properties and performance of PVDF VMD membranes, Desalination, (2015) 75–84.
[24] W. Hongxia, F. Jian, C. Tong, D. Jie, Q. Liangti, D. Liming, W. Xungai, L. Tong, One-step coating of fluoro-containing silica nanoparticles for universal generation of surface superhydrophobicity, Chem. Commun., 0 (2008) 877–879.
[25] J.A. Prince, G. Singh, D. Rana, T. Matsuura, V. Anbharasi, T.S. Shanmugasundaram, Preparation and characterization of highly hydrophobic poly(vinylidene fluoride) – Clay nanocomposite nanofiber membranes (PVDF–clay NNMs) for desalination using direct contact membrane distillation, J. Membr. Sci., 397– 398 (2012) 80–86.
[26] Y. Yang, D. Rana, T. Matsuura, S. Zheng, C.Q. Lan, Criteria for the selection of a support material to fabricate coated membranes for a life support device, RSC Adv., 4 (2014) 38711–38717.
[27] J.C. Mierzwa, C.D. Vecitis, J. Carvalho, V. Arieta, M. Verlage, Anion dopant effects on the structure and performance of polyethersulfone membranes, J. Membr. Sci., 421 (2012) 91–102.
[28] S. Zhao, Z. Wang, J. Wang, S. Wang, Poly (ether sulfone)/polyaniline nanocomposite membranes: effect of nanofiber size on membrane morphology and properties, Ind. Eng. Chem. Res., 53 (2014) 11468–11477.
[29] R. Sagar, B. Madhuleena, M. Somenath, Enhanced desalination via functionalized carbon nanotube immobilized membrane in direct contact membrane distillation, Sep. Purif. Technol., 136 (2014) 58–65.

[30] B.D. Jared, W.P. Gregory, Preparation of hydrophobic metal-organic frameworks via plasma enhanced chemical vapor deposition of perfluoroalkanes for the removal of ammonia, J. Vis. Exp., 80 (2013) e51175.
[31] N. Hering, K. Schreiber, R. Riedel, O. Lichtenberger, Woltersdorf, Synthesis of polymeric precursors for the formation of nanocrystalline Ti-C-N/amorphous Si-C-N composites, J. Appl. Organomet. Chem., 15 (2001) 879–886.
[32] A.Y. Jeong, S.M. Goo, D.P. Kim, Characterization of hydrophobic SiO_2 powders prepared by surface modification on wet gel, J. Sol–Gel Sci. Technol., 19 (2000) 483–487.
[33] T.H. Young, L.W. Chen, Pore formation mechanism of membranes from phase inversion process, Desalination, 103 (1995) 233–247.
[34] J.F. Li, Z.L. Xu, H. Yang, Microporous polyethersulfone membranes prepared under the combined precipitation conditions with non-solvent additives, Polym. Adv. Technol., 19 (2008) 251–257.
[35] H. Holmquist, S.I. Schellenberger, V. Vander, G.M. Peters, P.E.G. Leonards, Properties performance and associated hazards of state-of-the-art durable water repellent (DWR) chemistry for textile finishing, Environ. Int., 91 (2016) 251–264.
[36] B.J. Basu, T. Bharathidasan, C. Anandan, Superhydrophobic oleophobic PDMS-silica nanocomposite coating, ICE Sci., 1 (2013) 40–51.
[37] W. Chen, A.Y. Fadeev, M.C. Hsieh, D. Oner, Ultra hydrophobic and ultra-lyophobic surfaces: some comments and examples, Langmuir, 15 (1999) 3395–3399.
[38] M. Baghbanzadeh, A. Rashidi, A.H. Soleimanisalim, D. Rashtchian, Investigating the rheological properties of nanofluids of water/hybrid nanostructure of spherical silica/MWCNT, Thermochim Acta, 578 (2014) 53–58.
[39] D. Rana, T. Matsuura, Surface modifications for antifouling membranes, Chem. Rev., 110 (2010) 2448–2471.
[40] M. Younjin, A. Mustafa, K. Kai, G. Yuval, I. Jacob, The role of interparticle and external forces in nanoparticle assembly, Nature Mat., 7 (2008) 527–538.
[41] H.W. Sahng, P. Jinwon, R.M. Byoung, Relationship between permeate flux and surface roughness of membranes with similar water contact angle values, Sep. Purif. Technol., 146 (2015) 187–191.
[42] M.K. Souhaimi, T. Matsuura, Membrane distillation: Principles and applications, Elsevier, (2011) The Netherlands.